Neurocomputing 194 (2016) 326–339

Contents lists available at ScienceDirect

Neurocomputing

journal homepage: www.elsevier.com/locate/neucom

Union Laplacian pyramid with multiple features for medical image fusion

Jiao Du, Weisheng Li*, Bin Xiao, Qamar Nawaz

Chongqing Key Laboratory of Computational Intelligence, Chongqing University of Posts and Telecommunications, Chongqing 400065, China

ARTICLE INFO

Article history:
Received 15 July 2015
Received in revised form
18 February 2016
Accepted 20 February 2016
Available online 4 March 2016

Keywords:
Image fusion
Pyramid
Multiple features
Contrast enhancement
Outline enhancement
Objective image quality metrics

ABSTRACT

The Laplacian pyramid has been widely used for decomposing images into multiple scales. However, the Laplacian pyramid is believed as being unable to represent outline and contrast of the images well. To tackle these tasks, an approach union Laplacian pyramid with multiple features is presented for accurately transferring salient features from the input medical images into a single fused image. Firstly, the input images are transformed into their multi-scale representations by Laplacian pyramid. Secondly, the contrast feature map and outline feature map are extracted from the images at each scale, respectively. Thirdly, after extracting the multiple features, an efficient fusion scheme is developed to combine the pyramid coefficients. Lastly, the fused image is obtained by a reconstruction process of the inversed pyramid. Visual and statistical analyses show that the quality of fused image can be significantly improved over that of typical image quality assessment metrics in terms of structural similarity, peak-signal-to-noise ratio, standard deviation, and tone mapped image quality index metrics. The contrast is also well preserved by histogram analysis of images.

1. Introduction

The multi-modal medical image fusion is the process of merging multiple images from a single or multiple imaging modalities. The research of medical image fusion is focused on algorithms with aim to improve the imaging quality with preserving the specific features for increasing the clinical applicability of medical images for diagnosis and assessment of medical problems. Medical image fusion methods involve the fields of image processing, computer vision, pattern recognition, machine learning and artificial intelligence [1,2]. Thus far, medical image fusion methods can be implemented at three levels: pixel-level, feature-level and decision-level [3–5]. At the pixel-level of medical image fusion methods, most of the salient information is preserved in the fused image [3]. Feature-level image fusion methods [4] are performed on a feature-by-feature basis, such as edges, textures. And medical image fusion methods at the decision-level refer to make a final fused decision [5]. In this paper, we aim to generate a fused image combining the important information from multi-modal medical images at the pixel-level. Traditionally, the existing fusion methods can be summarized to implement by the following steps: image decomposition, image fusion rules, image reconstruction and image quality assessment [1,2]. Especially, the decomposition-based fusion methods decompose the input image into single-scale, two-scale or multi-scale sub-images.

At the pixel-level of medical image fusion methods, single-scale tools have been adopted for image fusion, e.g., fuzzy logic [6], knowledge [7], artificial neutral network (ANN) [8], principle component analysis (PCA) [9] and intensity hue luminance (IHS) [10] methods. Under the single-scale framework, the efficient image fusion rules are directly used to combine the input images with strategies to get the fused image. The fuzzy logic rule for each pixel in input images is utilized to uncertain reason for obtaining the final fused image [6]. In knowledge based method [7], both input medical images and medical reports are necessary to construct an image representation. In addition, ANN based method [8] applies the clustering method to divide the pixels into feature pixels and secondary pixels. PCA based method [9] is related to data-driven technique as well as higher order statistics to reveal hidden saliency structure. The fused image is constituted by new irrelevant principle components given by the convariance matrix of two decomposed coefficients. Then, IHS based method [10] is exposed to be a well quality images with a visually beautiful color medical images. The fused image is obtained by the substituted higher spatial resolution intensity component, original hue and saturation components.

The second category is the two-scale fusion methods, such as image fusion with guided filtering (GFF) [11]. Each input medical image is firstly decomposed into a base layer and a detail layer by average filter. Guided filtering is then performed on both base

* Corresponding author.
E-mail address: liws@cqupt.edu.cn (W. Li).

http://dx.doi.org/10.1016/j.neucom.2016.02.047
0925-2312/

layers and detail layers to get the fused layers which mean that the activity-level measurement of base layers is as same as detail layers. However, the guided filtering is good at blurring the image details while preserving the edges of the image. Since base layers represent the most information from the input images, maybe it is not fair to implement the guided filtering on the based layers to preserve the edge information but not the other significant information, such as texture information. Lastly, the fused image is obtained by combining the fused base layers and fused detail layers.

The last category is the multi-scale fusion methods. In the past few decades, many multi-scale geometric analysis (MGA) tools are adopted in the multi-modal image fusion and a large number of image fusion methods [12–25] with MGA have been proposed in literatures. MGA scheme can transfer the most important information of input multi-scale coefficients into the fused coefficients, such as pyramid transform (PT) [12–15], wavelet transform (WT) [16–25]. Specially, these PT MGA fusion methods include morphology pyramid [12], ratio pyramid (ROP) [13], Laplacian pyramid (LAP) [14], etc. And WT MRA fusion methods include discrete wavelet (DWT) [16,17], non-subsampled contourlet transform (NSCT) [22–24], and shearlet transform (ST) [25], etc. In MGA fusion methods, the multi-scale tool, transform is applied firstly to separate the input medical images into high resolution images and low resolution images. Image fusion rules are used to combine multiple high resolution images and low resolution images from different original input images, respectively. The fused high resolution images and fused low resolution images are then converted back into the fused image using the inverted transform. LAP [14] is formed as a difference between corresponding levels of the Gaussian and their expanded low-pass approximation images. NSCT [22–24] produces various directional decompositions due to non-subsampled directional filter bank. ST based decomposition methods [25] can capture more directional layers, compared with LAP, DWT, and NSCT. The average rule scheme for each pixel in input images is usually utilized in the low resolution images. Besides, a single feature is used to combine the high resolution images, such as max rule and local energy scheme. The computations of PT fusion [12–15] are relatively simple, however the WT fusion [16–25] provides result images at the express of considerably greater computation.

Although many advanced image fusion methods have been proposed in multi-modal medical image fusion applications, there still exists large room for improvement. In this study, we introduce a multiple features in LAP domain fusion method for multi-modal medical image fusion. The shortcoming of image fusion rules based on a single feature is to implement the same strategy in processing the residual-images from input images with different modalities. However, each image modality owns its properties. For example, anatomical image provides structural information, and functional image provides more activity of the tissues at the molecular level Maybe it is unfair to use a single feature extracted from input images. The proposed algorithm is to generate a multiple features of outline-enhanced and contrast-enhanced on the high resolution images to explore the properties from different medical images. The motivation of this fusion method is to combine the significant information of the high resolution images modeled as the outline and contrast enhancement by affine transformation [26,27], Kirsch scheme [28,29] and PCA [9]. The outline-enhance high resolution images is achieved using affine transformation [25,26] to enhance the edge information in horizontal and vertical orientations. And the contrast-enhance high resolution images is achieved using Kirsch scheme [28,29] and PCA [9]. The proposed fusion method in this paper is able to simultaneously combine the significant information of contrast-enhance, outline-enhanced. Therefore, multiple features are taken into consideration of fusing image in this paper. LAP is chosen as the decomposition and reconstruction scheme with the advantage that it can be implemented using simple image resizing routines in spatial domain. Outline weight map and contrast weight map are used to combine the decomposed high resolution images. Experimental results proved that our method is superior to the existing fusion approaches without loss of outline and color contrast. The study of this paper is:

1) The standard PT fusion method is directly transformed into several levels which are not capable to incorporate the detailed information. In this paper, the affine transformation is proposed to augment orientation information at each level.
2) Unlike the traditional PT method, the image fusion rule is inspired by the contrast and outline feature of the input images.
3) Designing multiple features for enhancing contrast and outline of images. The contrast information is attributed to Kirsch operator and PCA. And the outline information is extracted by affine transformation.

The rest of this paper is structured as follows: Section II gives a brief introduction of the pyramid transform based medical image fusion methods. Section III contains the details of the image fusion algorithm, and outline and contrast enhancement is provided. And Section IV discusses the image quality obtained with the proposed method by three groups of experiments of MRI-CT, MRI-PET, and MRI-SPECT fusion measurements. Finally, the conclusion is given in Section V.

2. A brief introduction of the pyramid transform fusion

The PT fusion methods include morphology pyramid (MOP) [12], ratio pyramid (ROP) [13], gradient pyramid (GRP) [12], and LAP [14]. The morphology filtered image is used to construct the high-pass frequency images in MOP based fusion methods. In ROP scheme, the ratio of adjacent image is applied to obtain the high-pass information. Moreover, GRP represents the high-pass frequency images by gradient of the corresponding images at different levels. Recently, LAP images are obtained as the difference between successive Gaussian filtered images using simple image resizing routines and smooth Gaussian kernels.

The PT fusion [12–15] mainly consists of three stages: image decomposition, image fusion and image reconstruction (shown in Fig. 1). PT is utilized to get the multi-scale representation of input images at the beginning. Secondly, the image at different scales is fused by efficient image rules. Finally, the fused image is obtained by the inversed PT. Please refer to Table 1 for important definitions used throughout the rest of this paper.

In Fig. 2, it is for the framework of a MRI image decomposition with three-level PT. A sequential order of images $\{L_1, L_2 \ldots L_i\}(i=3)$ is obtained by PT and the order is a couple of base-images B_i and residual images R_i. The base-images of the MRI image with three-levels are shown in Figs. 2 (b1), (c1), (d1). And the residual-images are shown in Figs. 2 (b2), (c2), (d2).

$$L_i = \begin{cases} \check{F} \times I, & i = 1 \\ \check{F} \times L_{i-1}, & 2 \le i \le n \end{cases} \tag{1}$$

where L_i is the i-th level, n is the maximum number of levels, $\check{F}$ is a filter with down-sampling and I is the input image.

The base-images B_i and residual-images R_i of L_i are obtained.

$$B_i = L_i \times F_L, \quad R_i = L_i \times F_H \tag{2}$$

where F_L is a low-pass filter, F_H is a high-pass filter.

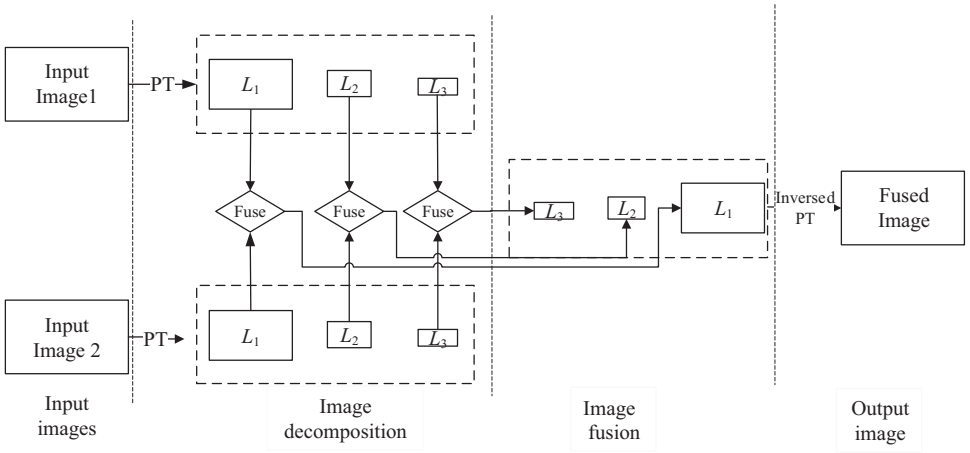

Fig. 1. Framework of three-levels pyramid transform based image fusion.

Table 1
Important notation and terms used in this paper.

$I, \bar{I}$	Image and mean value image.
C, D, F	Input image C, input image D, and fused image F respectively.
R, B	Residual image and base image.
F_L, F_H	High-pass and low-pass filter.
L	The decomposed image by pyramid at a given level
$\check{F}, \widehat{F}$	Down-sampling and up-sampling filter with value 2.
K	Image after Kirsch scheme.
A, A_1, A_2	Affine shear matrix, affine shear matrix in horizontal and vertical orientations.

Then, the fusion strategy in PT is at each level. For the base-images, the average scheme is chosen. As shown in Eq.(3), B'_i is the fused image at i-th level, B_i^1,B_i^2 are the two corresponding base-image at i-th level.

$$B'_i = \frac{1}{2} \times \left(B_i^1 + B_i^2\right) \tag{3}$$

In addition, the weight chosen for the residual-images is the maximum. R'_i is the fused image at i-th level, R_i^1,R_i^2 are the two corresponding residual-images.

$$R'_i = \begin{cases} R_i^1, & R_i^1 \geq R_i^2 \\ R_i^2, & else \end{cases} \tag{4}$$

Finally, image reconstruction is implemented by the inverse of image decomposition described above. The reconstruction equation is established as:

$$L'_{i-1} = \widehat{F} \times (L'_i + R'_i), i = 1, \ldots, n \quad \text{with} \quad L'_n = B'_n \tag{5}$$

where $\widehat{F}$ is a filter with sub-sampling, L_i' is the image at each level. The sequence of L_i' approximations is the base-image B_i' and residual-image R'_i.

3. Combinations of multiple features in pyramid transform domain

The proposed multiple feature fusion algorithm, which is based on the PT framework, is illustrated in Fig. 3. LAP transform is adopted as one of the PT tools for decomposing the input images into multi-scale image representation. An input image can be transformed into a series of residual-images and one approximate image by LAP. The approximate image provides the approximation of the input image. Moreover, the residual-images by LAP are obtained as the difference between successive Gaussian pyramid images using simple image resizing routines and smooth Gaussian kernels. The residual-images provide high-pass frequency saliency feature information from input medical images, such as edge information and texture information. The information from residual-images is significant for the quality of fused image. In many researching works, the papers emphasized on the fusion rules for the high-pass frequency images. Therefore, the multiple features is only utilized in the residual-images in order to preserve more significant information from medical images.

For notational simplicity, the R_i^1,R_i^2 are the residual-images at i-th level; R_{iH}^1, R_{iV}^1, R_{iH}^2, R_{iV}^2 are the residual-images in horizontal and vertical orientations; R_{iH}^o, R_{iV}^o, R_{iH}^c, R_{iV}^c are the contrast and outline features of residual-images in horizontal and vertical orientations respectively; R'_i is the fused image. The proposed algorithm is to generate an outline-enhanced and contrast-enhanced fused image based on LAP. By employment of affine transformation, the residual-images of two distinct images at the i-th level are decomposed into images in vertical and horizontal orientations. Then Kirsch [28,29] and PCA [9] features are applied to construct the contrast weight map. Moreover, the outline weight map is constructed via average of the images in vertical and horizontal orientations while preserving the most information of the residual-images at the i-th level. Finally, the fused residual-image at the i-th level is the combination of outline and contrast weight maps.

3.1. Affine transformation

Inspired by the matrix for controlling the orientation of ST coefficients [26,27], horizontal matrix $A_1 = [1, 0; 2, 1]$ and vertical affine matrix $A_2 = [1, 2; 0, 1]$ are used to separate each residual image into horizontal and vertical shear layers for preserving more edge information in details.

In ST, the shear matrix $A_1 = [1, \alpha; 0, 1](\alpha = 1)$ is used to construct the horizontal cone, and the shear matrix $A_2 = [1, 0; \beta, 1](\beta = 1)$ is used to construct the vertical cone. Therefore, we render these two matrixes on residual image at different scales for enhancing the edge in horizontal and vertical orientations in this paper. Especially, each pixel after the neighbor 2×2 filtering A_1 operation, the pixel value is the total of the pixels in the lower triangular. Compared with the original pixel, the gradient in horizontal orientation of the present pixel is larger. And each pixel after the filtering A_2, the pixel value is the total of the pixels in the upper triangular. The gradient in vertical orientation of the pixel with A_2 is larger than the original pixel. In other words, matrix A_1 and matrix A_2 are good at enhancing the edge of images in horizontal and vertical orientations, respectively.

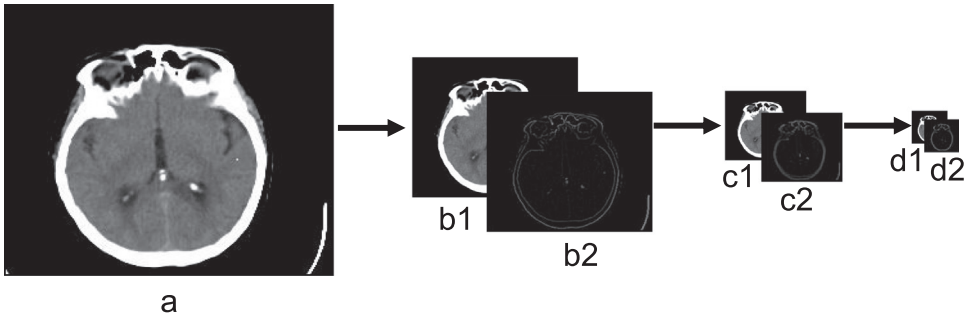

Fig. 2. Framework of a MRI image decomposition with three-level pyramid transform ((a) is the input image with MRI modality; (b1), (b_2) are the base-image and residual image respectively at the first level; (c_1), (c_2) are at the second level and (d_1), (d_2) are at the third level respectively.).

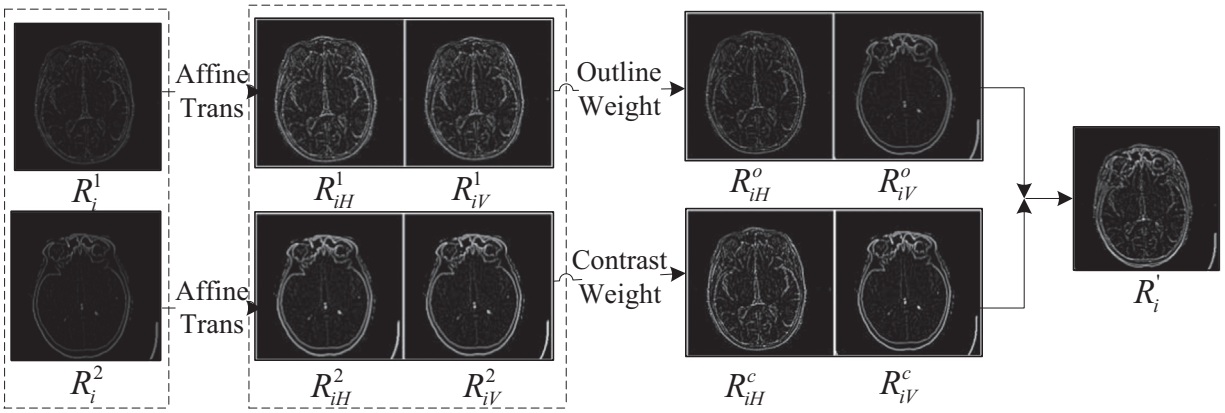

Fig. 3. Schematic diagram of the proposed multiple features fusion.

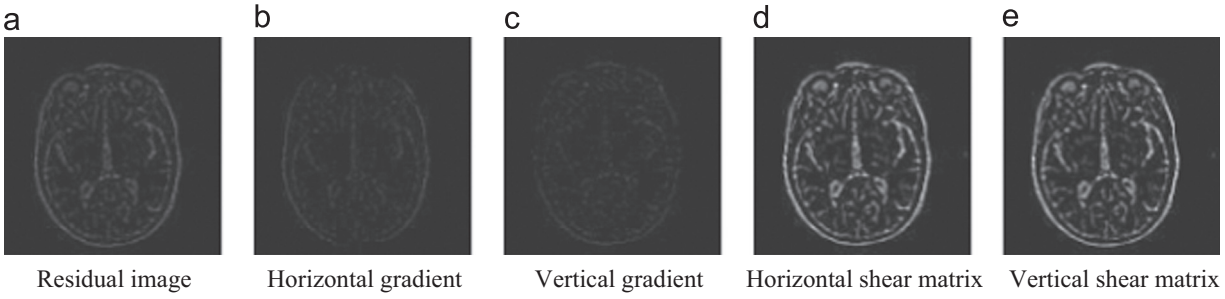

Fig. 4. Comparison between horizontal, vertical gradient and the proposed horizontal and vertical matrix images.

Fig. 4 illustrates the edge enhancement in horizontal and vertical orientations. Fig. 4. (a) is the processing original image. Residual image contains high resolution information, such as edge. The image after horizontal operation contains the signal changes in the horizontal orientation (see Fig. 4. (b) and (d)), while the vertical image contains vertical edges (see Fig. 4. (c) and (e)). Compared to the horizontal and vertical gradient, the shear matrix in ST performs better at enhancing the outline edge. Furthermore, Fig. 5. gives result images with different parameters (α, β) in shear matrix. The bigger the parameters, the clearer the edge in the image. In this paper, the default value setting is that $\alpha = 2$ and $\beta = 2$.

As shown in Fig. 3, the image fusion is firstly decomposed into horizontal and vertical orientations by affine transformation. This stage is given by 2-tuple $R_i = < R_{iH}, R_{iV} >$:

1) R_i: Residual-image at the i-th level.
2) R_{iH}: The residual-image in horizontal direction. The computation is $R_{iH} = R_i \times A_1$ where $A_1 = [1, 2; 0, 1]$.
3) R_{iV}: The residual-image in vertical direction. The computation is $R_{iV} = R_i \times A_2$ where $A_2 = [1, 0; 2, 1]$.

3.2. The contrast weight map

The contrast weight map is constructed by Kirsch feature [29] and PCA feature [9]. Kirsch feature is the representation of edge information. To take into account the differentiation of edge information in images, PCA, a statistical information about the multi-modal medical images, achieves that edge information of different images will contribute differently to the fused image.

Kirsch scheme [29] possess the characteristic of eight directions with different weight which is an operator for detecting the edges of images. The computation of eight edge directions is the convolution of template and each pixel value of the images. Due to the properties of preserving edge information, Kirsch is involved into this paper.

As shown in Fig. 3, the weight map of contrast enhancement is constructed as follows. First, residual-images R_{iH} and R_{iV} in horizontal and vertical orientation at i-th level are employed to obtain

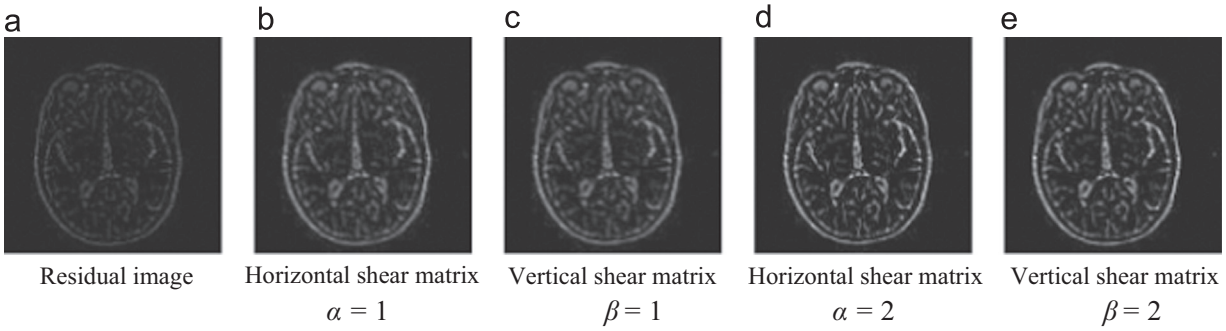

Fig. 5. Comparison between shearlet matrixes with different parameters.

the multi-resolution image K_{iH}, K_{iV} by Kirsch scheme.

$$K_{iH}=\frac{1}{8}\sum_{s=1}^{8}R_{iH}*w_s\ ,\ \ K_{iV}=\frac{1}{8}\sum_{s=1}^{8}R_{iV}*w_s \tag{6}$$

Where

$$w_1=\begin{bmatrix}5, & 5, & 5\\ -3, & 0, & -3\\ -3, & -3, & -3\end{bmatrix}, w_2=\begin{bmatrix}-3, & 5, & 5\\ -3, & 0, & 5\\ -3, & -3, & -3\end{bmatrix}, w_3=\begin{bmatrix}-3, & -3, & 5\\ -3, & 0, & 5\\ -3, & -3, & 5\end{bmatrix}, w_4=\begin{bmatrix}-3, & -3, & -3\\ -3, & 0, & 5\\ -3, & 5, & 5\end{bmatrix}$$
$$w_5=\begin{bmatrix}-3, & -3, & -3\\ -3, & 0 & -3\\ 5, & 5, & 5\end{bmatrix}, w_6=\begin{bmatrix}-3, & -3, & -3\\ 5, & 0, & -3\\ 5, & 5, & -3\end{bmatrix}, w_7=\begin{bmatrix}5, & -3, & -3\\ 5, & 0, & -3\\ 5, & -3 & -3\end{bmatrix}, w_8=\begin{bmatrix}5, & 5, & -3\\ 5, & 0, & -3\\ -3, & -3, & -3\end{bmatrix} \tag{7}$$

Since the principle of PCA [9] asserts that the eigenvalue is a measure of the primary feature in original images, it is a tool for enhancing images. The second step is the weight function which is obtained from multi-resolution image through processing Kirsch scheme by PCA, which projects the entire distribution of spectral values onto the line spanned by the eigenspace of the covariance matrix with largest eigenvalue.

Consequently, the weighted contrast maps R^c_{iH}, R^c_{iV} (as shown in Fig. 3) are obtained with Kirsch and PCA methods. The weighted images ensure that the regions with more saliency or high contrast from the input images. The two images by the two-stage framework are to construct a single image.

$$R^c_{iH}=K^1_{iH}\times m_1+K^2_{iH}\times m_2 \tag{8}$$

K^1_{iH}, K^2_{iH} are Kirsch scheme of the two model input image in horizontal orientation respectively. And m_1, m_2 are the PCA values of K^1_{iH}, K^2_{iH}.

$$m_1=\frac{E(1)}{\sum E}, m_2=\frac{E(2)}{\sum E} \tag{9}$$

where $E(1)$ and $E(2)$ are the eigenvalues of the covariance matrix K^1_{iH}, K^2_{iH}.

$$R^c_{iV}=K^1_{iV}\times n_1+K^2_{iV}\times n_2 \tag{10}$$

Similarly, the contrast weight map of two model input image K^1_{iV}, K^2_{iV} in vertical orientation is R^c_{iV}. And n_1, n_2 are the PCA values of K^1_{iV}, K^2_{iV}.

$$n_1=\frac{F(1)}{\sum F}, n_2=\frac{F(2)}{\sum F} \tag{11}$$

where $F(1)$ and $F(2)$ are the eigenvalues of the covariance matrix K^1_{iV},K^2_{iV}.

3.3. The outline weight map

For preserving more outline information, the mean value of the residual images with horizontal and vertical directions is to strengthen the outline of the images.

$$R^o_{iH}=\frac{1}{2}\left(\frac{1}{2}\left(R^1_i+R^2_i\right)+\frac{1}{2}\left(R^1_{iH}+R^2_{iH}\right)\right) \tag{12}$$

The horizontal orientation of images R^o_{iH} is obtained by the average of the residual-images R^1_i, R^2_i and its horizontal orientation R^1_{iH},R^2_{iH}.

$$R^o_{iV}=\frac{1}{2}\left(\frac{1}{2}\left(R^1_i+R^2_i\right)+\frac{1}{2}\left(R^1_{iV}+R^2_{iV}\right)\right) \tag{13}$$

For the vertical orientation of the images R^o_{iV}, the average strategy is used as well.

3.4. The combination of multiple features

Firstly, the contrast weight map R^c_i of the residual-images R_i at i-th level is obtained by Kritch and PCA.

$$R^c_i=\frac{1}{2}(R^c_{iH}+R^c_{iV}) \tag{14}$$

Secondly, the outline weight map R^o_i at i-th level is constructed by average.

$$R^o_i=\frac{1}{2}(R^o_{iH}+R^o_{iV}) \tag{15}$$

Finally, the combination scheme of residual-images R'_i (see Fig. 3) is the average of contrast and outline weight maps respectively written as

$$R'_i=\frac{1}{2}(R^c_i+R^o_i) \tag{16}$$

Similar to the traditional PT based image fusion algorithm, the steps of the combinations of multiple features based image fusion method can be listed as follows.

1) To apply the PT to each of the co-registered medical images and obtain a sequence of base-images and residual-images.

2) To combine the multiple features by Eq. (16) and get a fused residual-images at each layer. And the base-images at each layer are obtained by Eq. (3).
3) To use the inversed PT method by Eq. (5) to recover the fused image.

4. Experiments and discussion

4.1. Experimental setup

Experiments are implemented on the image database from the Whole Brain Web Site of the Harvard Medical School [30] which contains three groups of co-registered multi-modal images including MRI-CT, MRI-PET and PET-SPECT images. Each group owns two examples. The testing images have been used in many related papers [11–25]. The platform is MATLAB R2010b.

The proposed method is compared with seven image fusion approaches based on PCA [9], IHS [10], GFF [11], LAP [14], DWT [16], NSCT [22], and ST [25], respectively. The fusion strategies of these methods are illustrated underneath. The averaging scheme is adopted for the low-frequency bands of LAP, DWT, NSCT and ST approaches. Moreover, fusion strategies are adopted for the high-frequency bands of these three approaches. For LAP, high-pass frequency is to choose max. For DWT, the saliency features for combination the high-pass frequency. For NSCT, the max value with consistency check is to combine the high-pass frequency. In addition, the local energy scheme with the window size of 3×3 is used to combine the high-pass frequency obtained by ST.

4.2. Objective image quality assessment

Besides the subjective comparison, four objective image quality assessment metrics are adopted, i.e., structural similarity (*SSIM*) [31], peak-signal-to-noise ratio (*PSNR*) [32], standard-deviation (*STD*) [33] and tone mapped image quality index (*TMQI*) [34] metrics.

1) Structural similarity (*SSIM*) [31]
SSIM [31] is presented for full-reference image quality assessment with the assumption that human visual perception is highly adapted for extracting structural information. *SSIM* measures how well the structural information of input images is preserved

$$SSIM = \max(MSSIM_{C,F}, MSSIM_{D,F}) \tag{17}$$

where

$$\begin{cases} MSSIM_{C,F} = [l(C,F)]^a \cdot [c(C,F)]^b \cdot [s(C,F)]^c \\ MSSIM_{D,F} = [l(D,F)]^a \cdot [c(D,F)]^b \cdot [s(D,F)]^c \end{cases} \tag{18}$$

The task of *MSSIM* is separated into three components: luminance l, contrast c and structure s. Moreover, a, b and c are the constants with the same value of 1/3.

2) Peak-signal-to-noise ratio (*PSNR*) [32]
PSNR [32], derived from the information theory, reflects the quality of fused image without reference images and is defined as follows,

$$PSNR = \max(PSNR_{C,F}, PSNR_{D,F}) \tag{19}$$

3) Standard deviation (*STD*) [33]
STD [33] is simple and wide as an image quality metric. This metric defined with strict mathematical theory indicates the discreteness of distribution between the pixel values and the mean values.

$$STD = 1/(X \times Y) \sum_{x \le X, y \le Y} \left(F(x,y) - \overline{F}(x,y)\right)^2 \tag{20}$$

where $F(x,y)$ is the pixel value of the fusion image, $\overline{F}(x,y)$ is the average of the values and $X \times Y$ is the dimension, respectively.

4) Tone mapped image quality index (*TMQI*) [34]
TMQI [34] aims to measure the brightness and contrast between the input image and the fused image. In Eq. (13), S stands for the multi-scale structural fidelity and N is for statistical naturalness.

$$TMQI = 0.5 * (TMQI_{C,F} + TMQI_{D,F}) \tag{21}$$

where

$$TMQI_{C/D,F} = aS^{\alpha} + (1-a)N^{\beta} \tag{22}$$

The default values of parameters in *TMQI* are that $a = 0.8012$, $\alpha = 0.3046, \beta = 0.7088$.

4.3. Histogram analysis of images [35,36]

In addition to these four objective image quality assessments, image histogram is introduced as a new method for assessmenting the quality of images. Conventionally, the fused image resulting from different fusion methods is quantitatively compared with the arithmetic figures. However, image histogram is presented as a new image quality assessment to overcome the limitation of arithmetic figures. Image histogram can reflect the range of pixel values in the given image through the distribution curve graph in a two dimensional space. Image histogram is used to depict frequency of the image intensity values in an easily interpreted visual format. Traditionally, two kinds of histograms: intensity histogram and color histogram provide useful information, i.e., lighting, contrast and saturation effects for image components. In this paper, both intensity and color histograms have been applied as a metric for assessing the result images.

Firstly, the intensity histogram of a grey-level image is defined as follows,

$$P(n) = h(n)/N \tag{23}$$

where $h(n)$ is the number of pixels in the grey-level image with the intensity value n, N is the total number of pixel values. Secondly, the color histogram for color image contains three separate histograms, one each for the red, green and blue channels. Each histogram bin denotes the coarse distribution of the color information in an image.

4.4. Experiments results

Three groups of MRI-CT, MRI-PET and MRI-SPECT fusion experiments are implemented on MATLAB R2010b. The objective performances of different methods are evaluated with *SSIM*, *PSNR*, *STD* and *TMQI* metrics. In addition, the histogram analysis of images is applied to compare the contrast of fused images between the existing seven fusion methods and the proposed algorithm.

1) MRI-CT fusion

Fig. 6. and Fig. 7. show two examples of MRI-CT fusion, respectively. In Fig. 6. (a) and (b), it shows two source medical images captured by MRI and CT machine. Due to the different imaging principle, the first one display the soft issue structures in brain and another one reveals the bone structure with high

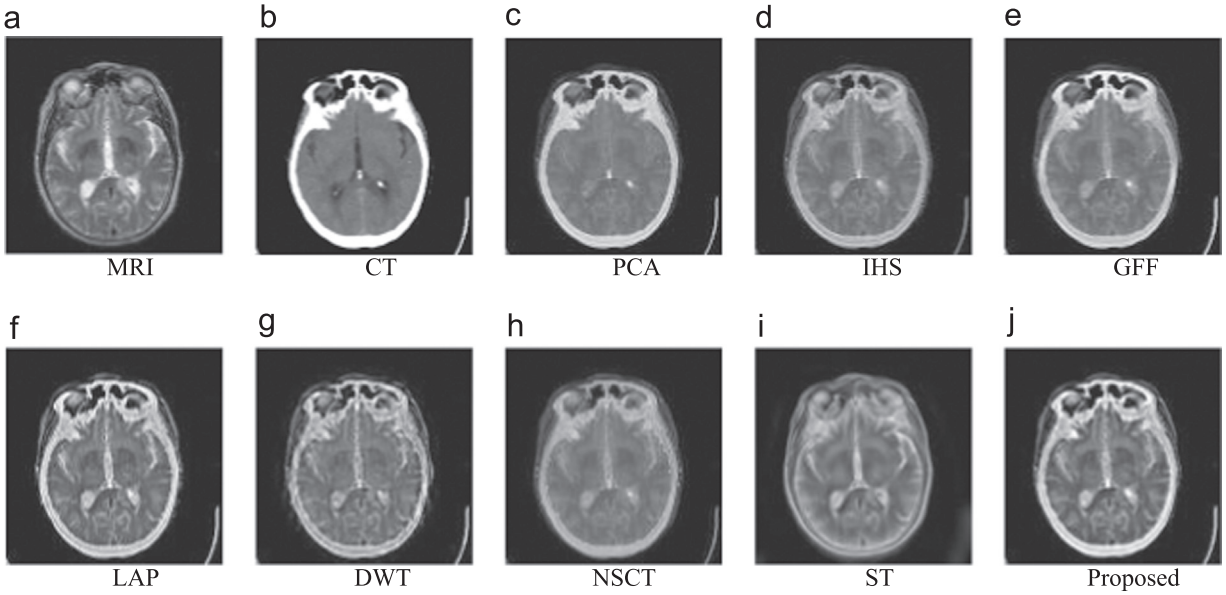

Fig. 6. Example 1: Performance comparison of different methods on MRI-CT fusion.

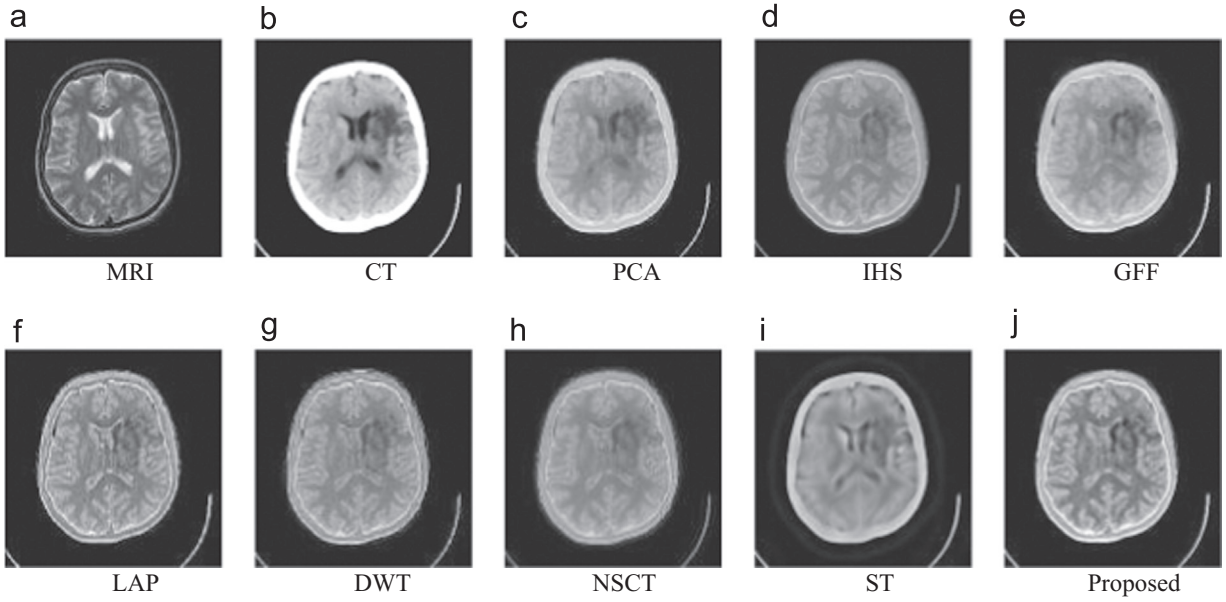

Fig. 7. Example 2: Performance comparison of different methods on MRI-CT fusion.

resolution. From Fig. 6. (c)-(j), it can be seen that the fusion images are produced by PCA, IHS, GFF, LAP, DWT, NSCT, ST and the proposed methods. As shown in Fig. 6. (c), (d) and (h), the PCA, IHS and NSCT based methods does not preserve the brightness of soft-tissue structures. The fused image is over-smoothed by the LAP based method (see Fig. 6. (f)). The DWT based method makes some edge information invisible (see Fig. 6. (g)). The result image by the ST based method provides very blurred outline. The GFF based method loses some important structure of brain (see Fig. 6. (e)). However, the brain structures are completely preserved by the proposed method, in Fig. 6. (j).

Similarly, Fig. 7. (a) and (b) show MRI and CT medical images. The black block in CT source image is preserved in the result images by PCA, GFF and proposed method (see Fig. 7. (c), (e) and (j)). On the other hand, the structural information, such as texture are perfectly preserved in the result images by LAP and the proposed method (see Fig. 7. (f) and (j)).

In addition, experimental results on four metrics are listed in Table 2–4. Table 2 shows that the proposed method obtains the highest value in terms of *STD* metric. Table 3 shows that the proposed method obtains the highest value in terms of *SSIM* and *TMQI* metrics. In other words, the proposed method specializes in preserving the structural and contrast information from different original images. Furthermore, Table 4 shows the average value of these four metrics. From Table 4, it can be observed that proposed method performs best in terms of *STD* metric. PCA based method performs best in terms of *SSIM* and *PSNR* metrics. Moreover, IHS based method performs best in terms of *TMQI* metric.

Furthermore, the histograms of final results by different fusion methods are listed in Fig. 8 and 9. In Fig. 8. (a) and (b), it can be seen that the curves of the two source gray-level images own a single peak. Looking at the curves of result images from PCA, IHS and NSCT based fusion methods, we see two distinct peaks. ST based fusion method provide large image range in the peak. LAP, GFF and

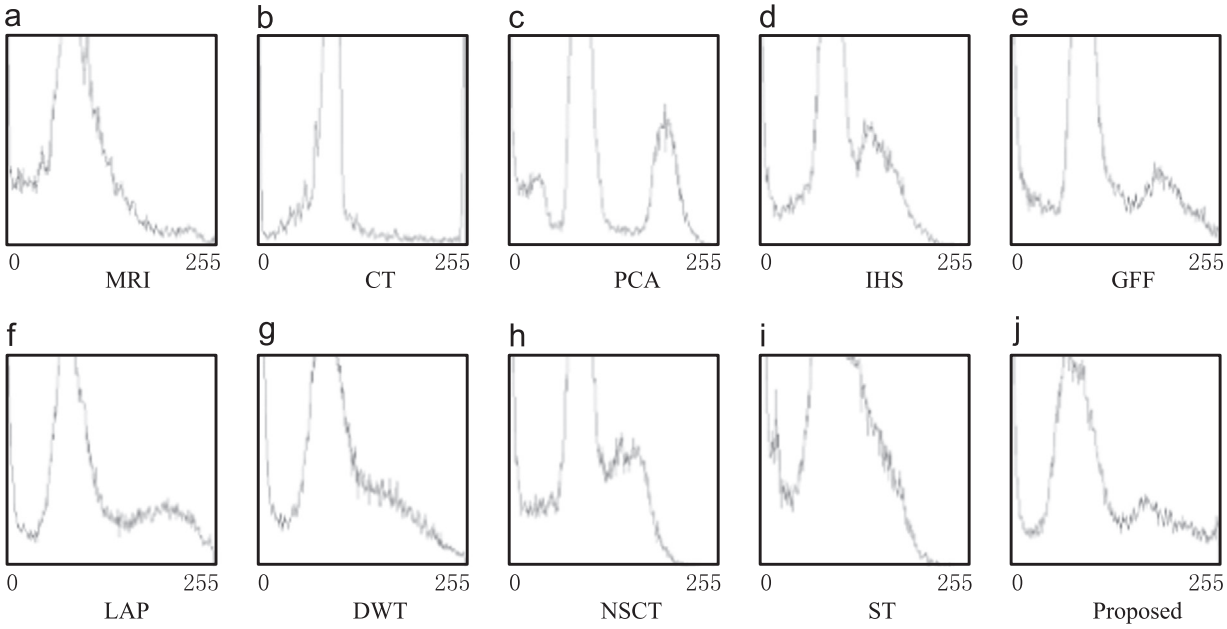

Fig. 8. Example 1: Histogram comparison of different fusion methods on MRI-CT fusion (The curve of gray is for the images.).

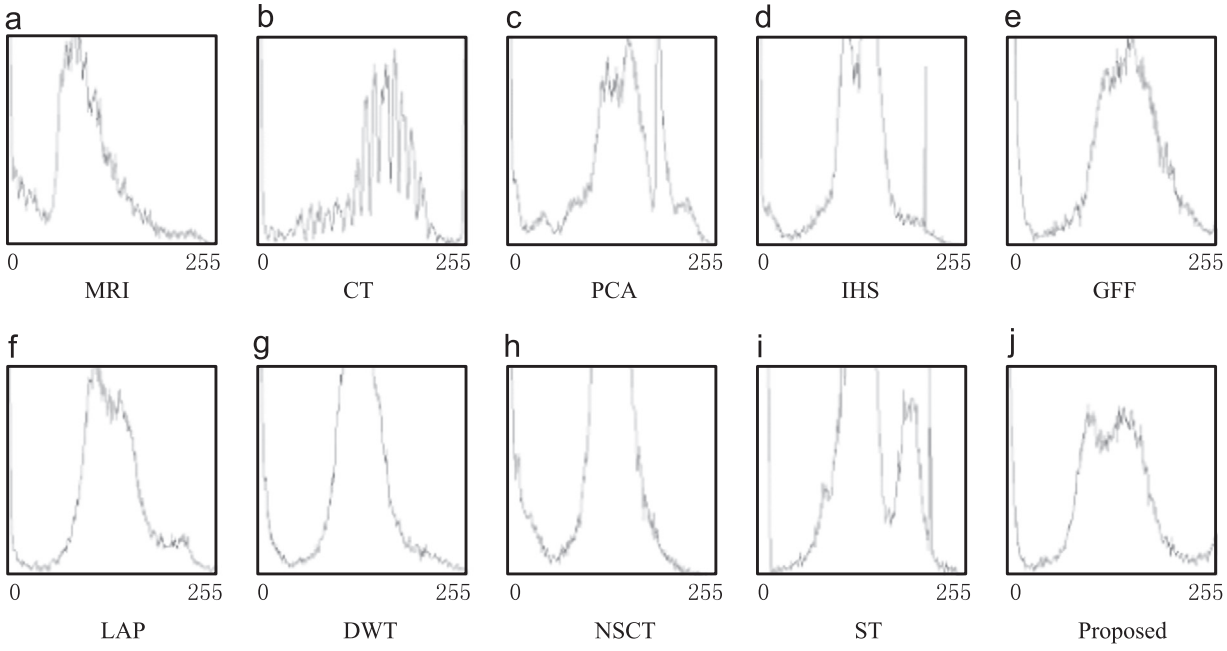

Fig. 9. Example 2: Histogram comparison of different fusion methods on MRI-CT fusion (The curve of gray is for the images.).

proposed methods provide the curve as same as the original source images. In Fig. 9. (j), the peak in the curve happen to correspond.

2) MRI-PET fusion

The MRI-PET fusion results are shown in Fig.10 and 11. Fig. 10. (a) and (b) show two modal images of MRI and PET. As shown in Fig. 10. (c), the PCA based method introduces color distortion. The fused images of IHS, GFF, DWT, and NSCT based methods show the low contrast (see Fig. 10. (d)–(e) and (g)–(h)). As shown in Fig. 10. (f), the LAP based method may lost the lesion region. The ST based method provide blur detail information. However, the proposed method preserves most of features and details from the original images (see Fig. 10.(j)).

Fig. 11 shows another example of MRI-PET fusion. PCA based method lost the white region, shown in Fig. 11. (c). IHS, GFF, DWT, and ST based methods lost luminance information, shown in Fig. 11. (d), (e), (g) and (i). However, the result image perfectly preserves the structural information.

Next, by the quantitative metrics in Table 5–7, the proposed method performs better than that of the PCA, IHS, LAP, DWT, NSCT, ST and GFF based methods. The *SSIM* metric gets better value by PCA based method than that of the proposed method. Furthermore, the proposed method performs best in terms of *PSNR*, *STD* and *TMQI* compared with the existing seven methods.

The histograms of different fusion methods are shown in Fig. 12 and 13. The valley of the curve is disappeared in the histogram of NSCT based method in Fig. 12. (h). In Fig. 12. (c), (f) and (j), the

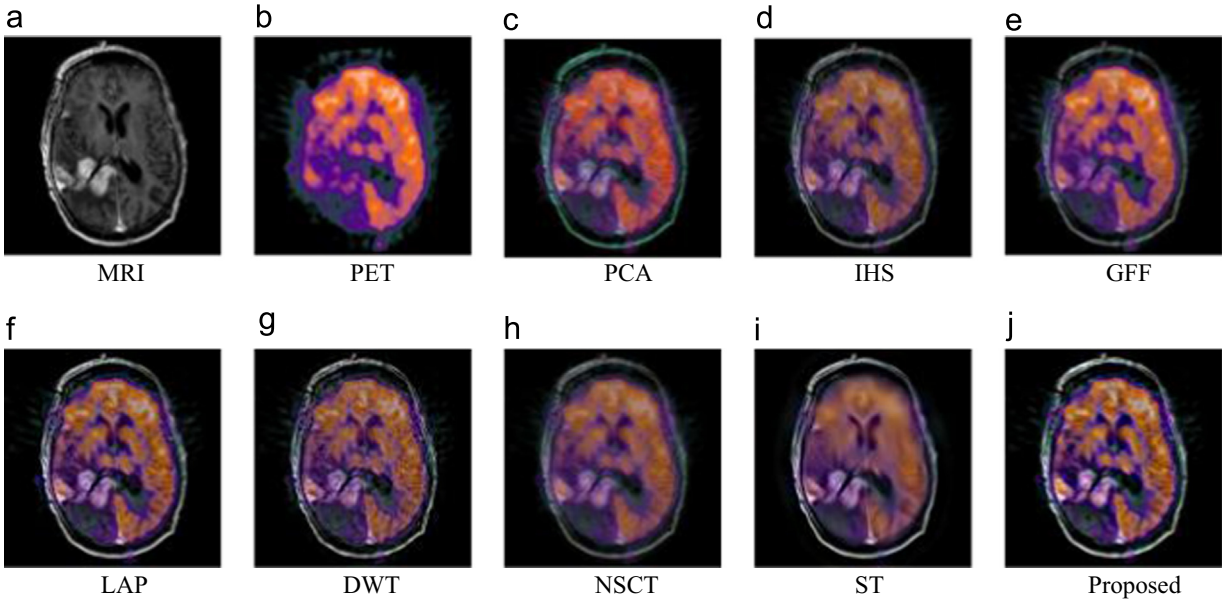

Fig. 10. Example 1: Performance comparison of different methods on MRI-PET fusion.

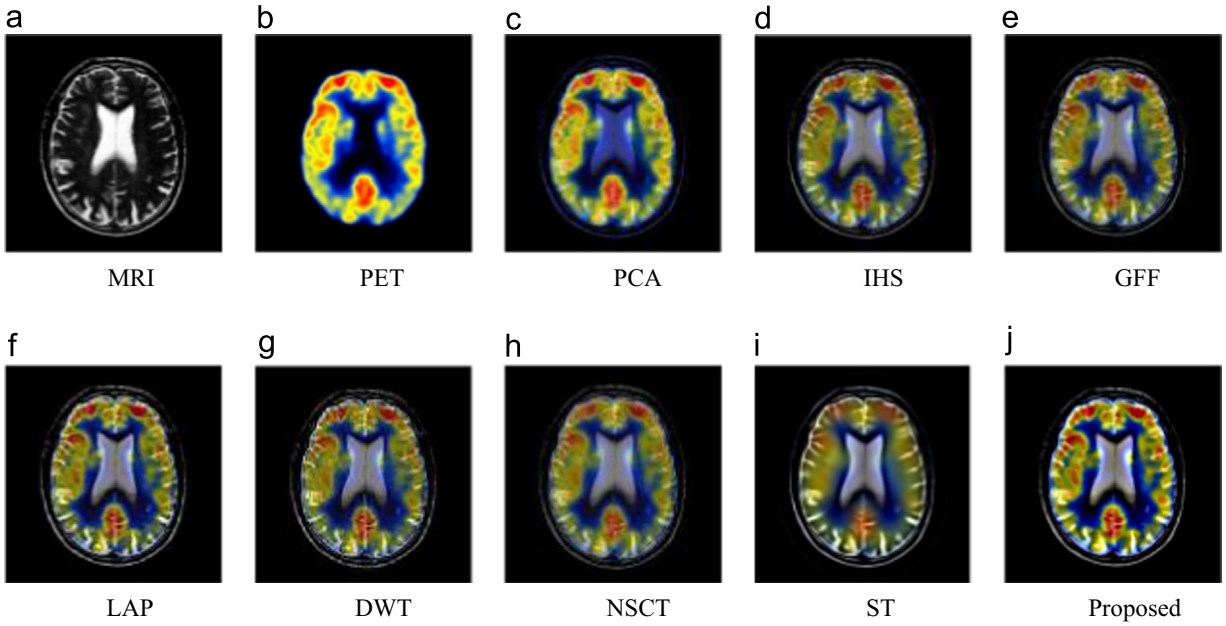

Fig. 11. Example 2: Performance comparison of different methods on MRI-PET fusion.

valley of the curve in original source PET image is perfectly retained in the final images by PCA, LAP and proposed fusion methods. By observing the curves in Fig. 13, the three distinct curves with red, green and blue color show a similar trend and smooth, obtained from proposed method.

3) MRI-SPECT fusion

The MRI-SPECT fusion results by PCA, IHS, GFF, LAP, DWT, NSCT, and the proposed method are shown in Fig. 14 and 15. Fig. 14. (a) and (b) show the original images pictured by MRI and SPECT. From Fig. 14. (c), PCA based method does not preserve the red region. The texture of brain structure in Fig. 12. (d), (g), and (h) looks blurring, but it appears clear in Fig. 14. (e) and (j). Next, another MRI-SPECT fusion example is presented in Fig. 15. As shown in Fig. 15. (c), the PCA based method introduces color distortion. The IHS based method does not work well in preserving functional information (see Fig. 15. (d)). As shown in Fig. 15. (f), (g) and (j), the result produced by the proposed method is much closer to the MRI and SPECT source images, whereas the results produced by other methods have low contrast around texture areas.

By comparing the quality metrics, the proposed method performs best in *STD* metric, shown in Table 5. That is, the outline information and edge information are reserved completely. For example 2, the proposed method performs best in terms of *PSNR* and *STD* metrics, shown in Table 6. At last, the objective performances of different methods are shown in Table 7. It can be seen that the proposed method performs best in *STD* metric.

In addition, the histogram comparison of different fusion methods is shown in Fig. 16 and 17. From Fig. 16. (a), it shows that abundant edge and structural information is abundant in MRI image. And high contrast information is plentiful in SPECT image. The histogram of the final result by proposed method in this paper

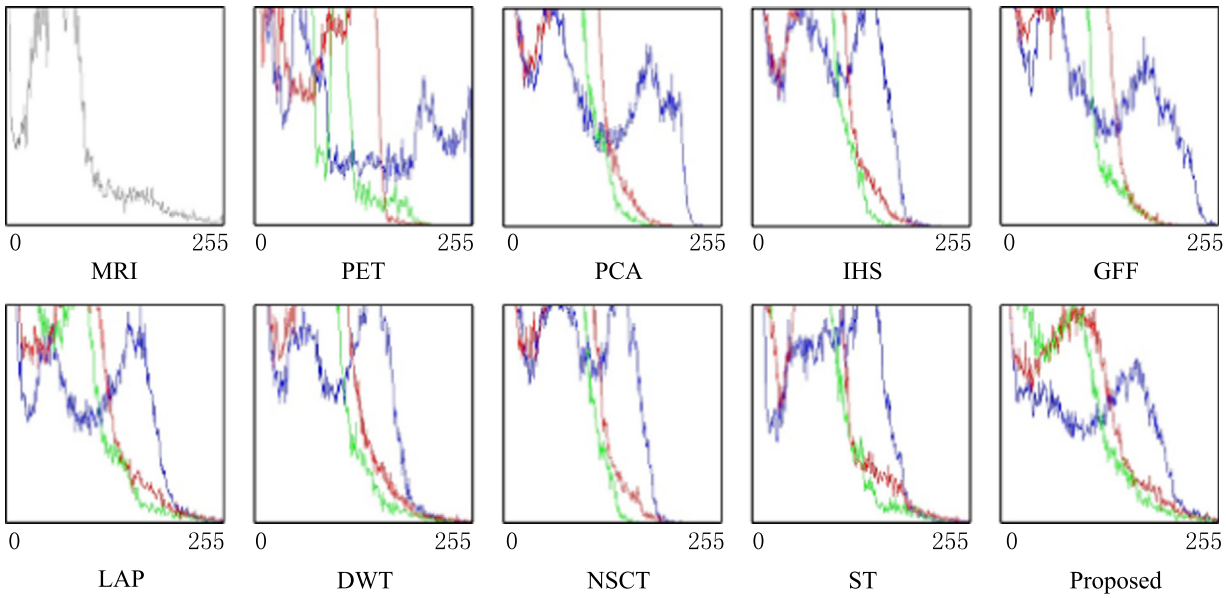

Fig. 12. Example 1: Histogram comparison of different fusion methods on MRI-PET fusion (Curves of red, green, blue are for the components of RGB color space.).

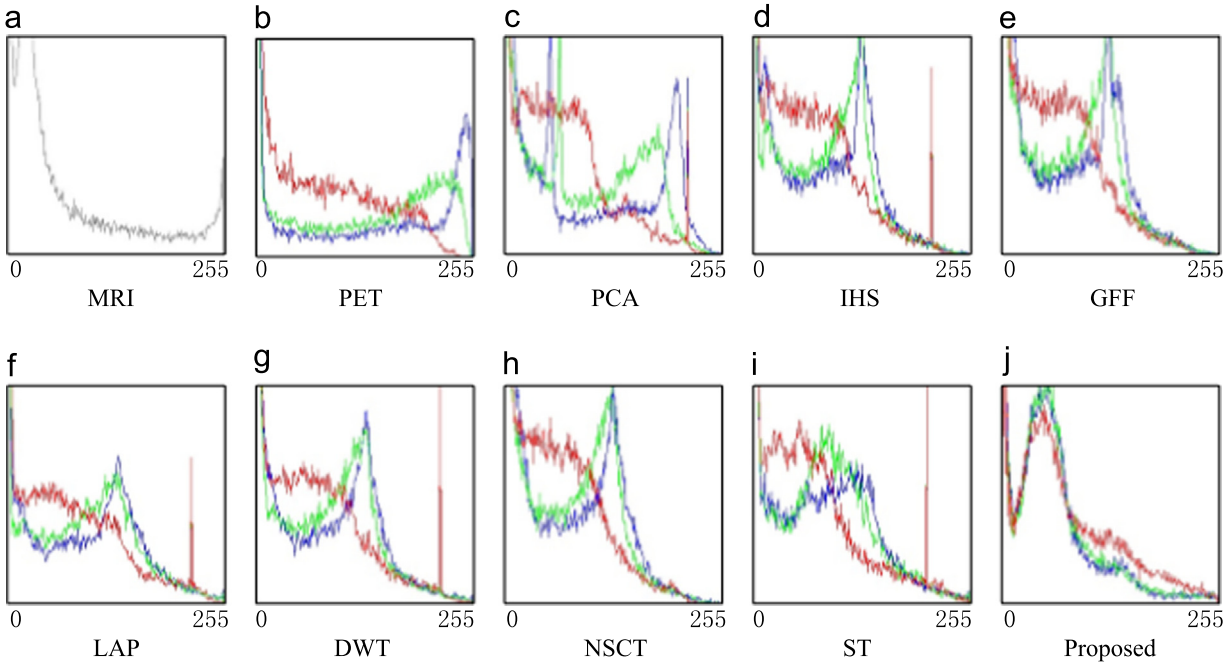

Fig. 13. Example 2: Histogram comparison of different fusion methods on MRI-PET fusion (Curves of red, green, blue are for the components of RGB color space.).

works well in transferring the high contrast information to the fused image, in Fig. 16. (j).

5. Conclusions

A PT based fusion method with multiple features is developed to preserve the outline and contrast information. The main part of the proposed approach is: 1) Input images: two multi-modal medical images. 2) Image decomposition: Multi-scale image representation is obtained by PT. 3) Image fusion: Weighted computing in each scale with the aim to enhance the outline and colure contrast. 4) Image reconstruction: the fused image is constructed by the inversed PT. 5) An output image: A single image to preserve the saliency features from two different medical modal images. Compared with the traditional methods such as PCA, IHS, GFF, LAP, DWT, NSCT, ST and the proposed method performs best in most image quality metrics. Furthermore, experiments show that the proposed method can well preserve edge information of multi-modal medical images. From the quantitative comparison results in Table 2–10, it can be clearly observed that the *SSIM*, *PSNR*, *STD* and *TMQI* metrics produce different ranking of these compared image fusion methods. In addition, image histogram is introduces as a new image quality assessment. From the image histograms described above, the histogram of the proposed image performs better compared with the other existing fusion methods.

However, all of these image fusion metrics can only measure the quality of fused images from a limited perspective, and it is difficult

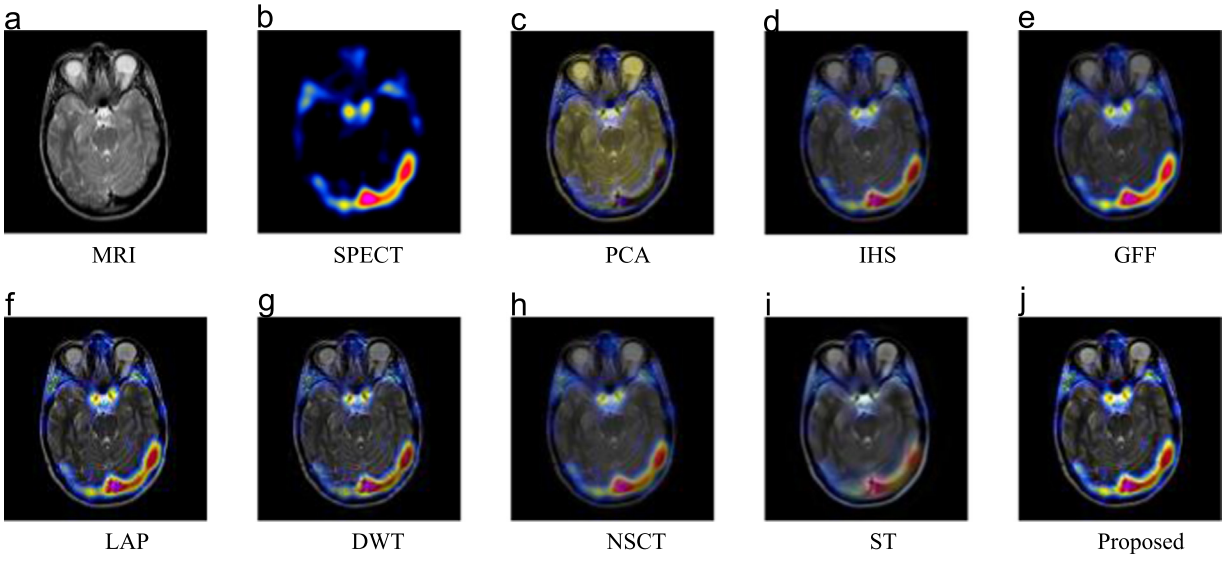

Fig. 14. Example 1: Performance comparison of different methods on MRI-SPECT fusion.

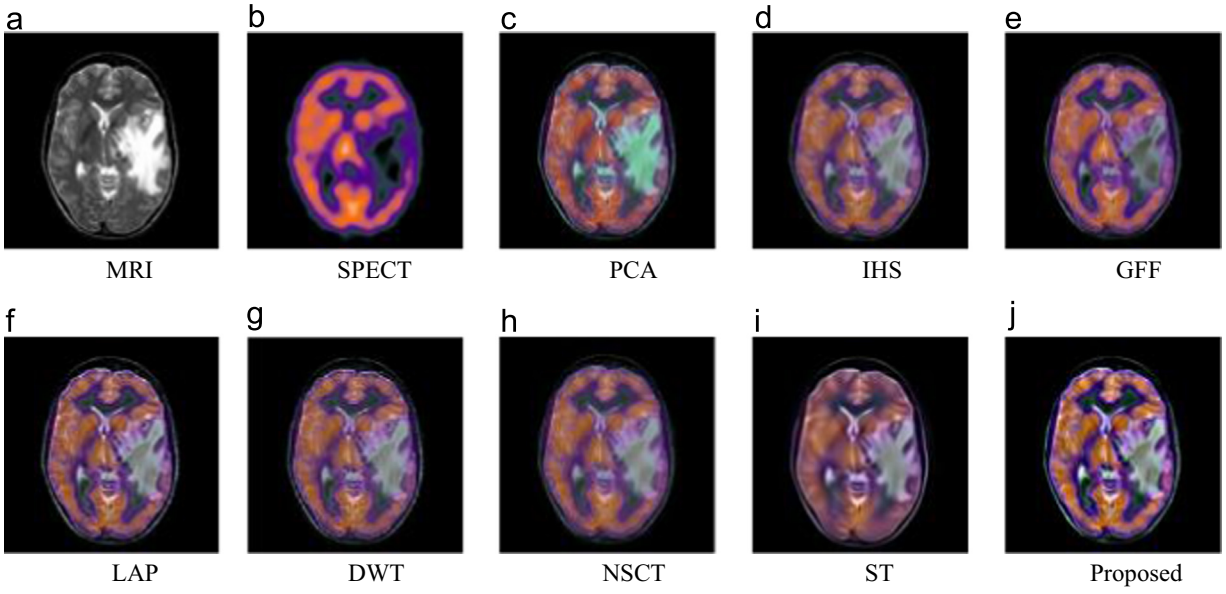

Fig. 15. Example 2: Performance comparison of different methods on MRI-SPECT fusion.

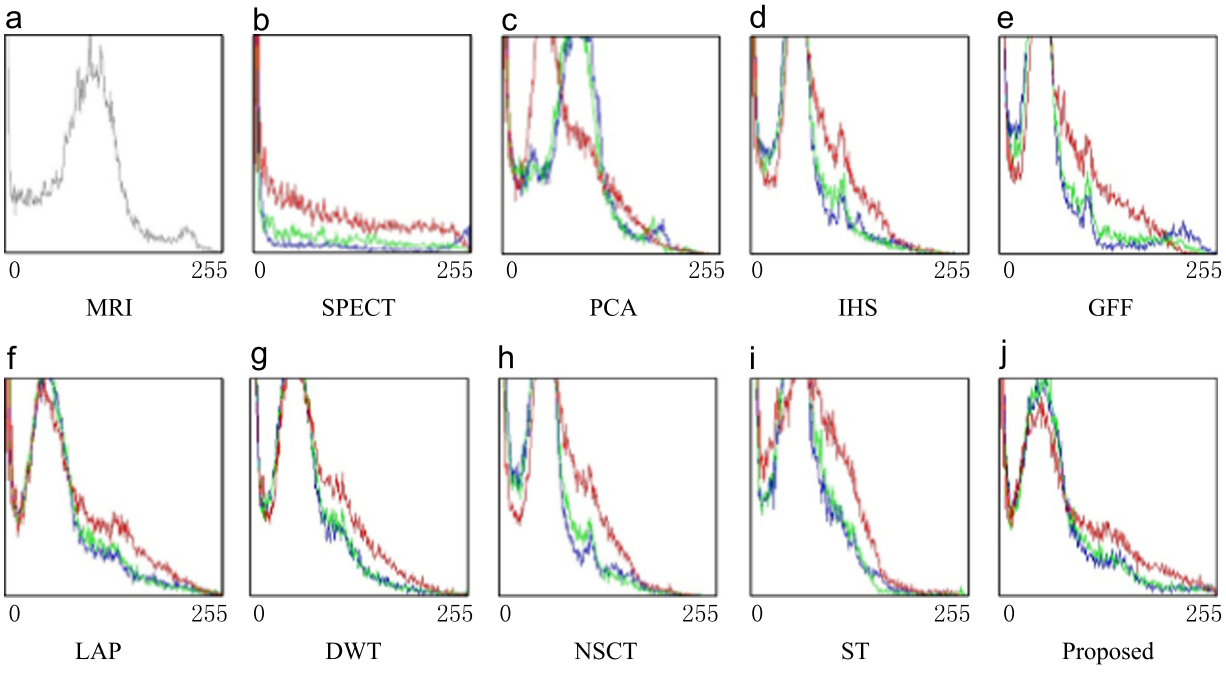

Fig. 16. Example 1: Histogram comparison of different fusion methods on MRI-SPECT fusion (Curves of red, green, blue are for the components of RGB color space.).

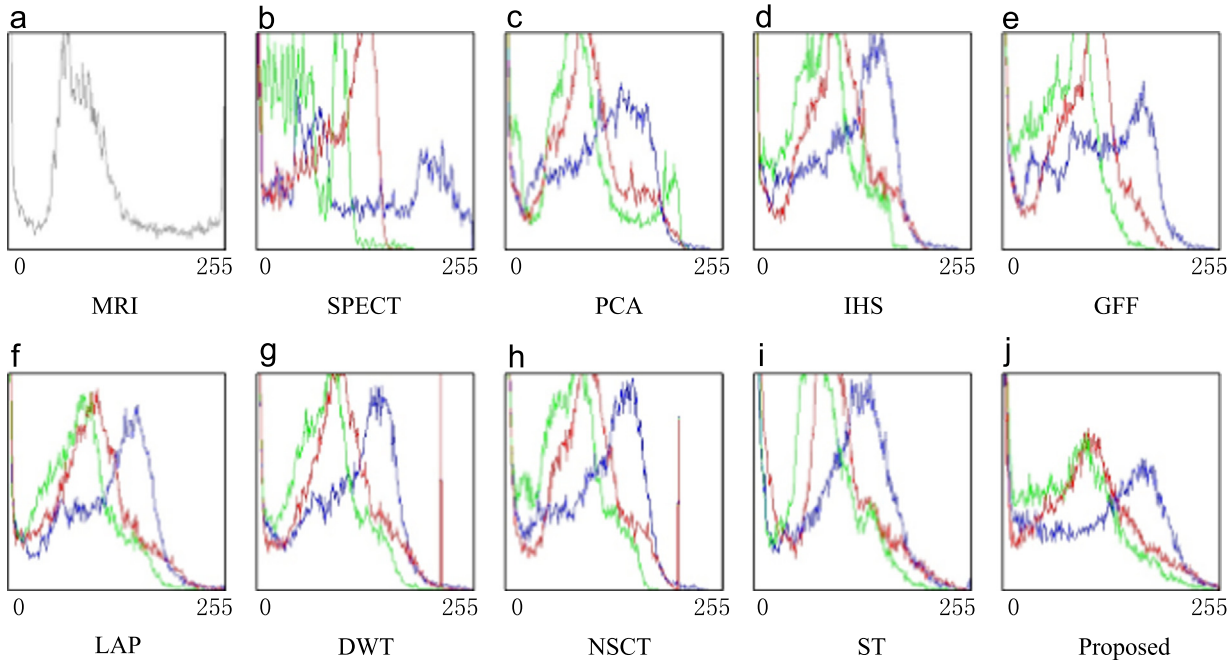

Fig. 17. Example 2: Histogram comparison of different fusion methods on MRI-SPECT fusion (Curves of red, green, blue are for the components of RGB color space.).

Table 2
Example 1: Comparison of MRI-CT fusion.

	SSIM	*PSNR*	*STD*	*TMQI*
PCA	**0.9337**	**20.8224**	1.2710	0.6944
IHS	0.8727	16.6220	1.1837	**0.7072**
GFF	0.9094	19.4033	1.2667	0.7038
LAP	0.8658	17.7271	1.3435	0.6933
DWT	0.8413	16.6171	1.2706	0.6954
NSCT	0.8571	16.3952	1.1631	0.6995
ST	0.9046	19.8395	1.1209	0.6542
Proposed	0.8513	17.3422	**1.3445**	0.6950

Table 3
Example 2: Comparison of MRI-CT fusion.

	SSIM	*PSNR*	*STD*	*TMQI*
PCA	1.2081	0.8520	18.8390	0.6890
IHS	1.1782	0.8595	15.1648	0.7213
GFF	1.2235	**0.8618**	**19.8143**	0.7134
LAP	1.2267	0.8247	14.6261	0.7169
DWT	1.1892	0.8258	14.9454	0.7207
NSCT	1.1477	0.8248	15.1845	0.7098
ST	1.2059	0.8141	18.0788	0.5866
Proposed	**1.2495**	0.8457	16.3914	**0.7232**

Table 4
MRI-CT fusion: Average value of metrics.

	SSIM	*PSNR*	*STD*	*TMQI*
PCA	**0.8929**	**19.8307**	1.2396	0.6917
IHS	0.8661	15.8934	1.1810	**0.7143**
GFF	0.8856	19.6088	1.2451	0.7086
LAP	0.8453	16.1766	1.2851	0.7051
DWT	0.8336	15.7813	1.2299	0.7081
NSCT	0.8410	15.7899	1.1554	0.7047
ST	0.8594	18.9592	1.1634	0.6204
Proposed	0.8485	16.8668	**1.2970**	0.7091

Table 5
Example 1: Comparison of MRI-PET fusion.

	SSIM	*PSNR*	*STD*	*TMQI*
PCA	0.9135	21.3797	1.1046	**0.7285**
IHS	0.8937	20.5039	1.0992	0.7284
GFF	**0.9309**	**22.5666**	1.0930	0.7151
LAP	0.9097	21.8434	1.2089	0.7240
DWT	0.8935	21.3288	1.1623	0.7245
NSCT	0.8955	20.0277	1.0829	0.7235
ST	0.9079	22.3008	1.1634	0.6934
Proposed	0.8924	20.4562	**1.2434**	0.7217

Table 6
Example 2: Comparison of MRI-PET fusion.

	SSIM	*PSNR*	*STD*	*TMQI*
PCA	**0.8643**	17.4075	1.4192	0.6722
IHS	0.8007	14.7456	1.3897	0.5063
LAP	0.7794	15.3367	1.4673	0.6894
DWT	0.7837	15.2137	1.4316	0.6888
NSCT	0.7870	15.5814	1.3467	0.6831
ST	0.8037	15.6148	1.4664	0.6675
GFF	0.8290	16.5302	1.3982	**0.7021**
Proposed	0.8060	**19.5018**	**1.5542**	0.6970

Table 7
MRI-PET fusion: Average value of metrics.

	SSIM	*PSNR*	*STD*	*TMQI*
PCA	**0.8889**	19.3936	1.2619	0.7004
IHS	0.8472	17.6248	1.2445	0.6174
LAP	0.8446	18.5901	1.3381	0.7067
DWT	0.8386	18.2713	1.2970	0.7067
NSCT	0.8413	17.8046	1.2148	0.7033
ST	0.8558	18.9578	1.3149	0.6805
GFF	0.8800	19.5484	1.2456	0.7086
Proposed	0.8492	**19.9790**	**1.3988**	**0.7094**

Table 8
Example 1: Comparison of MRI-SPECT fusion.

	SSIM	*PSNR*	*STD*	*TMQI*
PCA	**0.9501**	23.0871	1.2993	0.6686
IHS	0.8825	18.0259	1.3126	0.6960
GFF	0.8539	**16.6830**	1.3662	0.6922
LAP	0.8936	18.0739	1.4174	0.6927
DWT	0.8953	18.2583	1.3776	0.6919
NSCT	0.8672	17.8031	1.2949	**0.6949**
ST	0.8917	18.7915	1.3390	0.6724
Proposed	0.8662	17.5912	**1.4610**	0.6888

Table 9
Example 2: Comparison of MRI-SPECT fusion.

	SSIM	*PSNR*	*STD*	*TMQI*
PCA	**0.9287**	20.3231	1.2790	0.6974
IHS	0.8943	18.5302	1.2377	0.5792
GFF	0.9271	20.0603	1.2620	**0.7332**
LAP	0.9452	19.8649	1.3143	0.6102
DWT	0.8938	17.5383	1.2839	0.7077
NSCT	0.9084	17.9672	1.2527	0.7074
ST	0.8911	18.7956	1.2853	0.6839
Proposed	0.8948	**19.5018**	**1.3668**	0.7193

Table 10
MRI-SPECT fusion: Average value of metrics.

	SSIM	*PSNR*	*STD*	*TMQI*
PCA	**0.9394**	**21.7051**	1.2891	0.6830
IHS	0.8884	18.2781	1.2752	0.6376
GFF	0.8905	18.3717	1.3141	**0.7127**
LAP	0.9194	18.9694	1.3659	0.6515
DWT	0.8946	17.8983	1.3308	0.6998
NSCT	0.8878	17.8852	1.2738	0.7012
ST	0.8914	18.7936	1.3122	0.6782
Proposed	0.8805	18.5465	**1.4139**	0.7041

to distinct which objective metric is significantly better. For example, most of the objective metrics measure the structural information between the reference image and the result image. However, few metrics appear to measure the functional information. Later, researchers adopt no-reference image quality metrics into multi-modal medical image application. How to find the best suitable metric for the specific image processing application? For example, design a specific objective image quality assessment in the application of multi-modal medical image fusion. In this paper, we make a trial to apply image histogram to evaluate the image quality. But the effectiveness of image histogram is yield to testify using subjective assessments. In the future, we will make much more effort to design the metrics for evaluating functional information based on image histogram. Furthermore, adaptively choosing the different definitions for evaluating the image quality for different image processing applications is studied, as well. The challenges of designing a new objective image quality assessment are: prior knowledge from the clinical doctors is uncertain and several of diseases could not be judged by a unified form.

Acknowledgment

This work was supported in part by Natural Science Foundation of China (No.61272195, 61472055, U1401252), Program for New Century Excellent Talents in University of China (NCET-11-1085), Chongqing Outstanding Youth Fund (cstc2014jcyjjq40001) and Chongqing Research Program of Application Foundation and Advanced Technology (cstc2012jjA1699).

References

[1] A.P. James, B.V. Dasarathy, Medical image fusion: a survey of the state of the art, Inf. Fusion 19 (2014) 4–19.
[2] R. Shen, I. Cheng, A. Basu, Cross-scale coefficient selection for volumetric medical image fusion, IEEE Trans. Biomed. Eng. 60 (4) (2013) 1069–1079.
[3] G. Piella, A general framework for multiresolution image fusion: from pixels to regions, Inf. fusion 4 (4) (2003) 259–280.
[4] V.D. Calhoun, T. Adali, Feature-based fusion of medical imaging data, IEEE Trans. Inf. Technol. Biomed. 13 (5) (2009) 711–720.
[5] A. Madabhushi, S. Agner, A. Basavanhally, Computer-aided prognosis: predicting patient and disease outcome via quantitative fusion of multi-scale, multi-modal data, Comput. Med. imaging Graph. 35 (7) (2011) 506–514.
[6] J. Teng, S. Wang, J. Zhang, et al., 2010. Neuro-fuzzy logic based fusion algorithm of medical images, IEEE Image and Signal Processing 2010 3rd International Congress 4, pp. 1552–1556.
[7] M. Raza, I. Gondal, D. Green, et al., Classifier fusion to predict breast cancer tumors based on microarray gene expression data, knowledge-based intelligent information and engineering systems, Springer Berl. Heidelb. (2005) 866–874.
[8] Y. Wu, C. Wang, S.C. Ng, et al., Breast cancer diagnosis using neural-based linear fusion strategies, Neural Information Processing, Springer Berl. Heidelb. (2006) 165–175.
[9] W. Hao-quan, X. Hao, 2009. Multi-mode medical image fusion algorithm based on principal component analysis, IEEE Symposium on Computer Network and Multimedia Technology 2009, pp. 1–4.
[10] T.M. Tu, S.C. Su, H.C. Shyu, et al., A new look at IHS-like image fusion methods, Inf. fusion 2 (3) (2001) 177–186.
[11] S. Li, X. Kang, J. Hu, Image fusion with guided filtering, IEEE Trans. Image Process. 22 (7) (2013) 2864–2875.
[12] A. Toet, Hierarchical image fusion, Mach. Vision. Appl. 3 (1) (1990) 1–11.
[13] A. Toet, Image fusion by a ratio of low-pass pyramid, Pattern Recognit. Lett. 9 (4) (1989) 245–253.
[14] P.J. Burt, E.H. Adelson, The Laplacian pyramid as a compact image code, IEEE Trans. Commun. 31 (4) (1983) 532–540.
[15] V.S. Petrovic, C.S. Xydeas, Gradient-based multiresolution image fusion, IEEE Trans. Image Process. 13 (2) (2004) 228–237.
[16] Q. Guihong, Z. Dali, Y. Pingfan, Medical image fusion by wavelet transform modulus maxima, Opt. Express 9 (4) (2001) 184–190.
[17] R. Singh, M. Vatsa, A. Noore, 2009. Multimodal medical image fusion using redundant discrete wavelet transform, IEEE Seventh International Conference on Advances in Pattern Recognition, pp. 232–235.
[18] Y. Liu, J. Yang, J. Sun, 2010, PET/CT medical image fusion algorithm based on multiwavelet transform, IEEE 2010 2nd International Conference on Advanced Computer Control 2, pp. 264–268.
[19] W. Xue-jun, M. Ying, 2010. A Medical image fusion algorithm based on lifting wavelet transform, IEEE 2010 International Conference on Artificial Intelligence and Computational Intelligence 3, pp. 474–476.
[20] X. Li, X. Tian, Y. Sun, et al., Medical image fusion by multi-resolution analysis of wavelets transform, Wavel. Anal. Appl, Birkhäuser Basel (2007) 389–396.
[21] Q.P. Zhang, M. Liang, W.C. Sun, 2004, Medical diagnostic image fusion based on feature mapping wavelet neural networks, 2004 IEEE First Symposium on Multi-Agent Security and Survivability, pp. 51–54.
[22] G. Bhatnagar, Q.M. Wu, Z. Liu, Directive contrast based multimodal medical image fusion in NSCT domain, IEEE Trans. Multimed. 15 (5) (2013) 1014–1024.
[23] T. Li, Y. Wang, Biological image fusion using a NSCT based variable-weight method, Inf. Fusion 12 (2) (2011) 85–92.
[24] Y. Liu, S. Liu, Z. Wang, Medical Image Fusion by Combining Nonsubsampled Contourlet Transform and Sparse Representation, Pattern Recognit., Springer Berl. Heidelb. (2014) 372–381.
[25] Q. Miao, Q.C. Shi, P. Xu, et al., A novel algorithm of image fusion using shearlets, Opt. Commun. 284 (6) (2011) 1540–1547.
[26] G. Easley, D. Labate, W.Q. Lim, Sparse directional image representations using the discrete shearlet transform, Appl. Comput. Harmon. Anal. 25 (1) (2007) 25–46.
[27] Q. Wang Lim, The discrete shearlet transform: a new directional transform and compactly supported shearlet frames, IEEE Trans. Image Process. (2010).
[28] R. Kirsch, Computer determination of the constituent structure of biological images, Comput. Biomed. Res. 4 (1971) 315–328.
[29] C.I. Gonzalez, J.R. Castro, P. Melin, 2015. Cuckoo search algorithm for the optimization of type-2 fuzzy image edge detection systems, 2015 IEEE Congress on Evolutionary Computation (CEC), pp. 449–455.
[30] K. A. Johnson, J. A. Becker, The whole brain altas [Online], Available: ⟨http://www.med.harvard.edu/aanlib/⟩.
[31] Z. Wang, A.C. Bovik, H.R. Sheikh, et al., Image quality assessment: from error visibility to structural similarity, IEEE Trans. Image Process. 13 (4) (2004) 600–612.
[32] Z. Wang, Q. Li, Information content weighting for perceptual image quality assessment, IEEE Trans. Image Process. 20 (5) (2011) 1185–1198.
[33] Y. Liu, S. Liu, Z. Wang, A general framework for image fusion based on multi-scale transform and sparse representation, Inf. Fusion 24 (2015) 147–164.
[34] H. Yeganeh, Z. Wang, Objective quality assessment of tone-mapped images, IEEE Trans. Image Process. 22 (2) (2013) 657–667.

[35] Y. Xiao-Hu, J. Li-Cheng, Fusion algorithm for remote sensing images based on nonsubsampled contourlet transform, Acta Autom. Sin. 34 (3) (2008) 274–281.
[36] J. Han, K.K. Ma, Fuzzy color histogram and its use in color image retrieval, IEEE Trans. Image Process. 11 (8) (2002) 944–952.

Jiao Du was born in Chongqing, P.R. China, in 1988. She received M.S. degree from Chongqing University of Posts and Telecommunications, Chongqing, P.R. China. Currently, she is a Ph.D. candidate in computer science and technology, with the Chongqing Key Laboratory of Computational Intelligence, Chongqing University of Posts and Telecommunications. Her research interests include pattern recognition and image processing.

Weisheng Li graduated from School of Electronics & Mechanical Engineering at Xidian University, Xi'an, China in July 1997. He received M.S. degree and Ph.D. degree from School of Electronics & Mechanical Engineering and School of Computer Science & Technology at Xidian University in July 2000 and July 2004, respectively. Currently he is a professor of Chongqing University of Posts and Telecommunications. His research focuses on intelligent information processing and pattern recognition.

Bin Xiao was born in 1982. He received his B.S. and M. S. degrees in Electrical Engineering from Shaanxi Normal University, Xian, China in 2004 and 2007, received his Ph. D. degree in computer science from Xidian University, Xi'an, China. He is now working as an associate professor at Chongqing University of Posts and Telecommunications, Chongqing, China. His research interests include image processing, pattern recognition and digital watermarking.

Mr. Qamar Nawaz had earned his degree of MS (Computer Science) from The University of Agriculture, Faisalabad, in 2008. He joined the same university in 2008 to extend his services in teaching as well as application development domain. Currently, he is a PhD student in the department of computer science, Chongqing University of Post and Telecommunication. His research area is image processing.